Non-Astigmatic Alexandrite Ring Laser Design with Wavelength-tunable Single-Longitudinal-Mode operation

JUNA SATHIAN,[1,2,*] GORONWY TAWY,[1] XIN SHENG,[1] ARA MINASSIAN,[3] AND MICHAEL J. DAMZEN[1]

[1]*Photonics Group, The Blackett Laboratory, Department of Physics, Imperial College London, Prince Consort Road, London SW7 2AZ, UK*
[2]*Department of Mathematics, Physics and Electrical Engineering, Northumbria University, Newcastle upon Tyne NE1 8ST, UK*
[3]*Unilase Ltd, 60 Grays Inn Road, Unit LG04, London WC1X 8AQ, UK*
**juna.sathian@northumbria.ac.uk*

Abstract: This work presents a study of a fully non-astigmatic design of a single-longitudinal-mode, wavelength-tunable, unidirectional Alexandrite ring laser cavity and assessment of its performance compared to more complex laser design requiring astigmatism compensation. A "displaced mode" non-astigmatic laser cavity design eliminating astigmatic cavity elements is developed around an Alexandrite crystal end-pumped by a low brightness high power red diode laser pump system. Single-longitudinal-mode, continuous-wave operation is demonstrated with output power 700 mW with an excellent TEM_{00} mode (M^2 <1.1) across a wide pump power range. Wavelength tuning from 748-773 nm is produced using a birefringent filter plate. The non-astigmatic Alexandrite laser design achieves better spatial quality and resilience to maintain TEM_{00} operation across wide variation in pump-induced lensing compared to the astigmatic design. To the best of our knowledge, this is the first wavelength-tunable, single-longitudinal-mode operation of a unidirectional Alexandrite ring system in a fully non-astigmatic cavity regime.

1. Introduction

Alexandrite [Chrysoberyl ($BeAl_2O_4$) doped with Chromium ions (Cr^{3+})] is a broadly tunable (701-858 nm) solid-state vibronic laser. Its broad tunability combined with excellent thermo-mechanical properties for high power and long upper-state lifetime for good energy storage makes Alexandrite an interesting laser material for many applications including medical [1], high-resolution spectroscopy [2], and remote sensing/lidar [3]. Alexandrite lasers operate well at room-temperature and, interestingly, performance improves at elevated temperature [4-6] due to enhanced effective gain cross-section. This contrasts to most solid-state lasers such as Nd:YAG and Ti:Sapphire, which perform better when cooled. Three-level laser operation at ~680 nm is also possible from the ^2E storage level and enhanced performance at this transition has been shown at cryogenic temperatures [7]. Alexandrite has broad absorption bands across the visible spectrum, which allows various pump schemes such as flash lamps, arc lamps or laser diodes [4-8]. Development of Alexandrite lasers with direct red diode-pumping is of prime interest due to small quantum defect, high system efficiency and low cost. First demonstrations of red diode-pumped Alexandrite were by Scheps in the early 1990s [9,10]. In more recent years, advancement in high power red diode lasers (Aluminum Gallium Indium Phosphide, AlGaInP), has enabled more efficient and multi-watt diode-pumped operation of side-pumped Alexandrite slab lasers [11], a record power of 26.2 W in end-pumped Alexandrite rod configuration using free-space diode pumping [12], fibre-delivered diode end-pumped Alexandrite laser with the highest slope efficiency to date (54%)

[13], and utilising the long upper-state lifetime for energy storage, Q-switched operation of diode-pumped Alexandrite has been demonstrated [11,12,14].

Whilst several Alexandrite laser demonstrations have been made in recent years by a few research groups, for future precision applications in areas such as quantum technologies and remote sensing there is the additional need for Alexandrite to operate with an ultra-narrow linewidth (MHz or sub-MHz) and with precise wavelength selectivity for spectral locking to narrow atomic/molecular transitions [2,3,14]. First demonstrations of narrow linewidth development have been made in an injection-seeded unidirectional Alexandrite ring laser in Q-switched pulse mode for atmospheric lidar at the potassium resonance at 770 nm [14], and in a wavelength-tunable unidirectional continuous-wave single-longitudinal-mode Alexandrite laser [15]. These first demonstrations have had to address issues with asymmetrically-shaped pumping [14] and astigmatic cavity elements (Brewster-cut laser crystal and angled curved mirrors) [15] requiring bespoke cavity designs with astigmatism compensation to enable high quality TEM_{00} operation in both the horizontal and vertical mode directions. A further significant issue encountered is the asymmetric pumping, which is especially pronounced in Brewster-cut crystal even for symmetric pump beam, leading to astigmatic pump-induced lensing and restricting the stable TEM_{00} operational power range [15] without making complex cavity adjustments. Therefore, although astigmatism compensation laser schemes have been devised [15-20], and beam symmetrising by using fibre-delivery of pump [21], there is still a challenge for design complexity when using astigmatic cavity elements and limitations for laser operating power variation [14,15].

This paper reports a systematic laser development of a non-astigmatic Alexandrite ring laser design with no astigmatic elements. The aim was to compare operation of the non-astigmatic Alexandrite ring laser to a more complex bow-tie ring cavity design incorporating Brewster-angle cut Alexandrite crystal and angled curved cavity mirrors configured for astigmatism compensation [15]. The outcome of this study is the successful operation of a compact unidirectional non-astigmatic Alexandrite ring laser design with single-frequency operation and superior TEM_{00} spatial quality across a much wider pump range.

In Section 2, a compact two-mirror laser cavity is operated to calibrate maximum efficiency of a plane-plane parallel cut non-astigmatic Alexandrite crystal end-pumped by a moderate-power fibre-delivered red diode pump module, which is then developed into a non-astigmatic rectangular-shaped ring laser cavity design and operated in bidirectional mode. In Section 3, a full detailing is made of ring resonator "displaced mode" TEM_{00} design using ABCD cavity modelling software and finite element analysis (FEA) to optimise under varying pump-dependent thermal lensing. Experimentally, the non-astigmatic ring laser system is operated in unidirectional mode and with a higher-power free-space red diode pump module. Continuous-wave, unidirectional Alexandrite ring cavity operation is obtained in single-longitudinal-mode (SLM) with output power of 700 mW at a wavelength of 754.6 nm and excellent TEM_{00} beam quality M^2_x (horizontal) × M^2_y (vertical) = 1.07 × 1.06. Using a birefringent filter, wavelength tuning of the unidirectional ring cavity was achieved from 748 nm to 773 nm, with tuning limited by the spectral reflectivity of the output coupler. Section 4 provides final conclusions of the paper.

2. Alexandrite compact linear and bidirectional ring lasers with fibre-delivered diode pump

2.1 Compact linear Alexandrite laser

Before proceeding to the ring laser cavity design, a preliminary compact laser experiment was conducted on the diode-pumped performance of the Alexandrite crystal to be used in the ring cavity design. Figure 1 shows the end-pumped Alexandrite rod crystal in a compact plane-plane mirror cavity. The Alexandrite rod was a *c*-axis cut crystal with plane parallel end faces anti-reflection coated (at 755 nm) with length 10 mm, diameter 4 mm and with 0.22 at. % Cr doping concentration. The Alexandrite rod was embedded in water-cooled copper

heatsink at 16°C and mounted with its *b*-axis orientated horizontally in the cavity. The cavity consisted of a back mirror (BM) highly reflecting (R >99.9%) at laser wavelength (~755 nm) and highly transmitting (R <0.2%) for pump (~637 nm) and an output coupler (OC) with reflectivity R=98.8% at the laser wavelength. The cavity length was 16 mm.

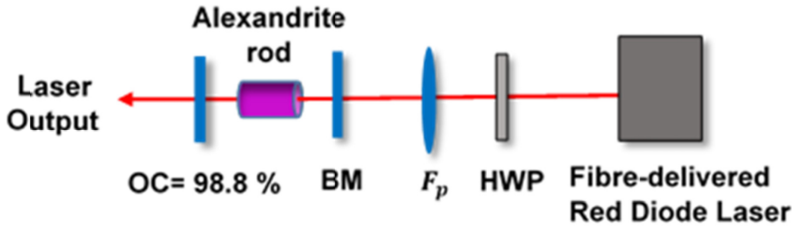

Fig.1. Schematic of compact diode end-pumped Alexandrite rod laser with BM = back mirror, OC = output coupler, F_p = pump beam focusing lens and HWP = half-wave plate for diode pump.

A fibre delivered red diode module, operating nominally at central wavelength 637 nm with a bandwidth (FWHM) of 1.5 nm, was used as an optical pump for the Alexandrite crystal. The diode multi-mode fibre had a core diameter of 105 µm and numerical aperture of 0.22. The output of the diode fibre was coupled to an aspheric lens fibre collimator with a focal length of 35 mm and then to an aspheric lens (F_p) with a focal length of 50 mm to focus the pump beam to a spot on the front face of the Alexandrite crystal with a measured beam waist radius of 70 µm and beam quality factor $M^2_x \times M^2_y = 49 \times 48$. The polarization of the pump module was only partially scrambled by the fibre with ~70% power in one axis that was oriented parallel to the b-axis of the Alexandrite rod with a half-wave plate (HWP) for maximum absorption.

Figure 2 shows the output power of the compact Alexandrite cavity as a function of absorbed pump power. The maximum power was 1.07 W at 3.4 W absorbed pump power with laser slope efficiency of 35% and threshold pump power 0.6 W. Beam quality measurements were made using ISO standard D4-sigma method showing the output was TEM_{00} with excellent beam quality $M^2_x \times M^2_y = 1.02 \times 1.04$. The laser results validate the good quality of the Alexandrite laser crystal for this study, and the feasibility for high diode-pumped operational efficiency.

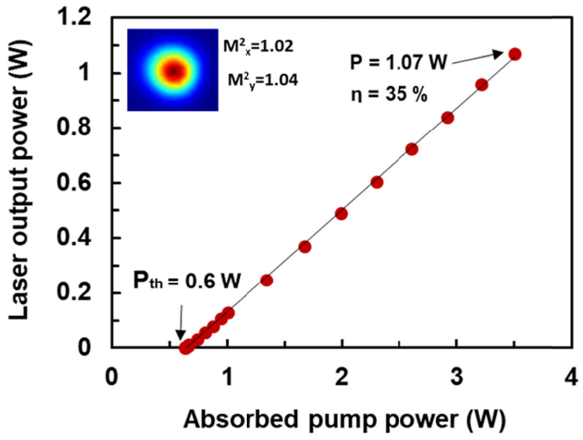

Fig. 2. Compact diode-pumped Alexandrite laser output against absorbed pump power.

2.2 Ring Alexandrite laser cavity

A stigmatic Alexandrite ring laser was formed using only non-astigmatic cavity elements and with a rectangular-shaped cavity as shown in Fig. 3 (a) around the plane-plane Alexandrite laser rod of the compact cavity. The cavity used three 45° mirrors (M1, M2, M3), which were highly reflecting (R>99.9%) for laser wavelength and highly transmitting for diode pump wavelength (~637 nm), and an output coupler, OC with reflectivity ~99.7%. Two intracavity plano-convex lenses L1 and L2 with focal length f =100 mm and antireflection coating at 755 nm (R<0.1%) were used at normal incidence in the cavity. The rectangular cavity shape (rather than bow-tie or otherwise) was chosen as it allowed best separation of cavity arms so that intracavity lenses (and later other components) could be mounted without collision of optics holders even in the small total cavity length 388 mm used, and for simplicity of lens translation direction. The lenses were chosen to have equal focal length for simplicity of understanding the cavity design. It is noted that the Alexandrite rod and lenses are used at normal incidence, so there is no astigmatism in these cavity elements, allowing much simpler laser design than the astigmatic cavity [15] as further detailed in Section 3.

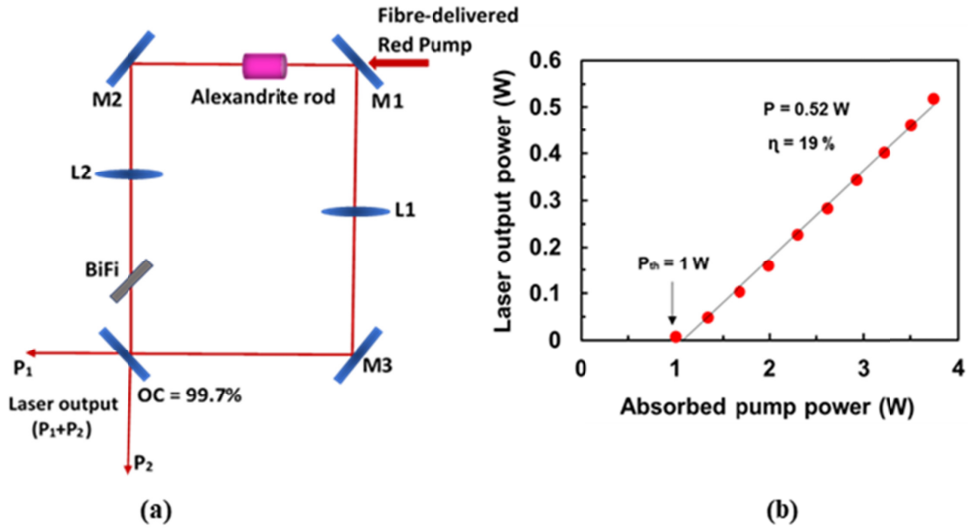

Fig. 3. (a) Ring cavity design and (b) laser output power against absorbed pump power for ring-shaped Alexandrite laser. The calculated slope efficiency is 19%.

The laser cavity operated bidirectionally with two outputs with powers P_1 and P_2 as shown in Fig. 3 (a). Figure 3 (b) shows total laser output power (P_1+P_2) as function of absorbed pump power, at an optimum crystal temperature 40°C. Maximum laser output power was 0.52 W, with laser slope efficiency of 19% and threshold pump power 1.0 W. The spatial output was TEM_{00} with excellent beam quality factor M^2_x =1.09 and M^2_y =1.06. The increased pump threshold indicates higher intracavity losses than the compact laser cavity even with the higher reflectivity of the ring output coupler.

Wavelength tuning of the bidirectional ring laser cavity was achieved by inserting a 1 mm thick quartz birefringent filter (BiFi) plate at Brewster angle to minimize insertion losses. The thin plate adds minimal astigmatism to the cavity. Figure 4 (a) shows wavelength tuning results between 739.5 nm and 782.2 nm, and Fig. 4 (b) shows the peak wavelength 755.3 nm whose spectral linewidth was below instrument-limited resolution ~0.5 nm of the spectrometer used.

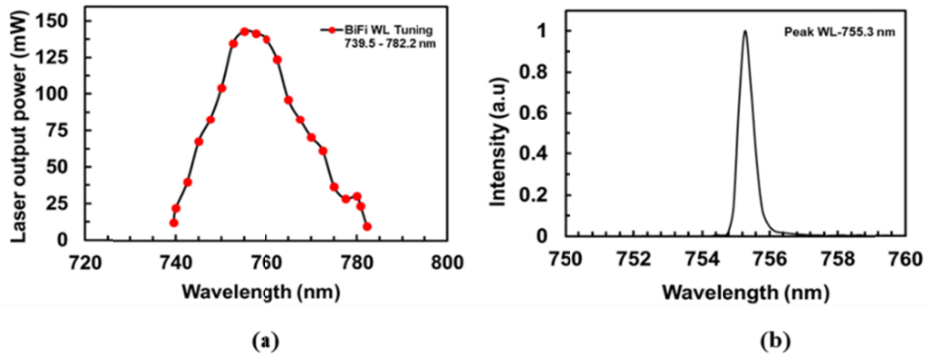

Fig. 4. (a) Wavelength tuning curve and (b) (instrument-limited) spectrum at peak wavelength of bidirectional diode-pumped Alexandrite non-astigmatic ring laser.

The fibre-delivered diode pump module used to demonstrate the non-astigmatic ring Alexandrite laser is too low in power to effectively show the potential of the unidirectional ring when further intracavity losses are introduced by the optical isolator system. To this end, a higher power free-space red diode pump module was utilised. This free-space multi-bar red diode pump with spatial-filtering to improve its spatial quality employed the same system used in prior Alexandrite laser work [15] where more details are given. The diode pump system provided 10.8 W of linearly polarized light at 638 nm with spatial quality M^2_x =60 and M^2_y =40. A half-wave plate was used to orient the pump light parallel to the high absorbing *b*-axis of the Alexandrite rod. The diode pump was focused at the input face of the Alexandrite rod to a beam waist radius w_x =70 µm and w_y =63 µm. Figure 5 shows bidirectional output power (P_1+P_2) as a function of absorbed pump power for the bidirectional Alexandrite ring laser when using an output coupler with reflectivity 99.2%. An output power of 1.16 W was produced with a 18.8% slope efficiency and output wavelength 758 nm.

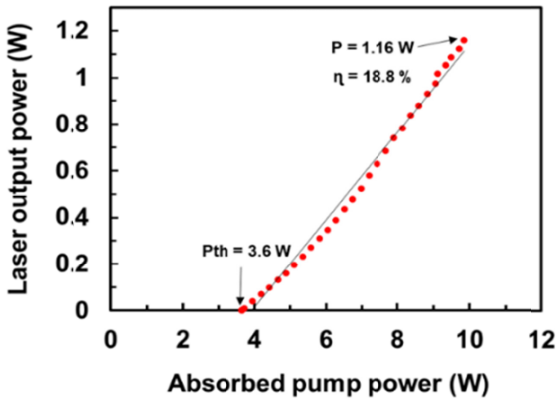

Fig. 5. Bidirectional ring laser output power versus absorbed pump power with 99.2 % output coupling at an emission wavelength of 758 nm.

3. Unidirectional Alexandrite ring laser design and operation

This section describes the unidirectional operation of the non-astigmatic Alexandrite ring laser using the 10.8 W free-space pump module and its numerical design modelling. Figure 6 shows the unidirectional non-astigmatic ring Alexandrite laser where a Faraday rotator (FR) and half-wave plate (HWP) are introduced to form an optical diode for the unidirectional ring operation (output direction P_1).

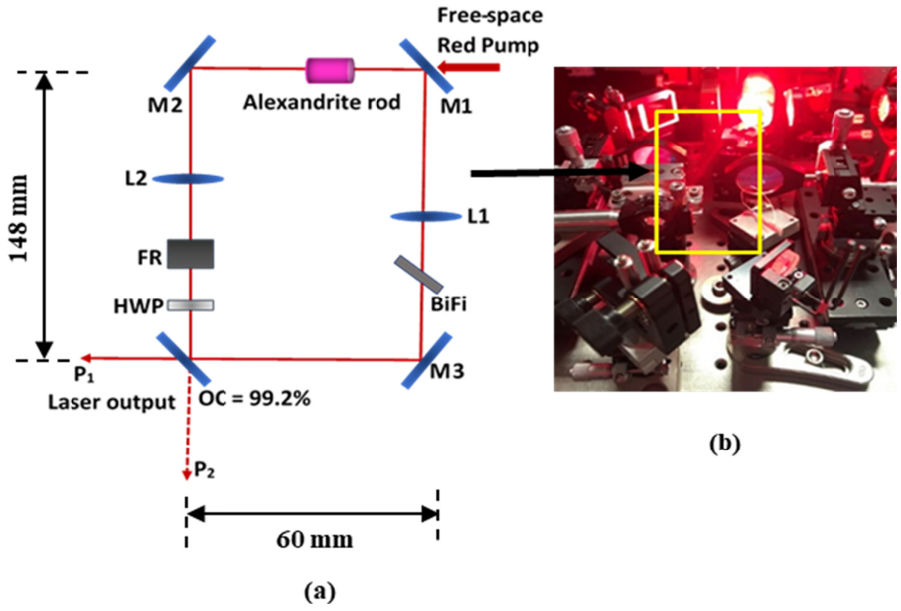

Fig. 6. Non-astigmatic unidirectional diode-pumped Alexandrite ring laser with optical diode composed of Faraday rotator (FR) and half-wave plate (HWP): (a) schematic and (b) photograph of system.

3.1 Numerical modelling of Alexandrite ring laser design

A resonator design strategy for achieving TEM_{00} operation was developed for the rectangular-shaped ring cavity with two intracavity lenses L1 and L2 with focal length 100 mm. The lens positions were adjustable to produce a small waist near the laser crystal with design target to form a spatial laser mode matching in size to the diode pump for TEM_{00} with account of the pump-induced lens in the Alexandrite crystal [15]. The laser cavity design for the TEM_{00} non-astigmatic Alexandrite ring laser was developed using the Laser Cavity Analysis and Design (LASCAD®) software for ABCD Gaussian beam propagation modelling combined with a Finite Element Analysis (FEA) to compute the thermally induced lensing effect in the end-pumped Alexandrite laser crystal.

Pump-induced thermal effects in the diode pumped Alexandrite crystal are detrimental since a power dependent lensing is produced, changing the beam propagation parameters and stability of the laser cavity, affecting power range for TEM_{00} operation and beam quality degradation due to the aberrating nature of the thermal lens. In the FEA results for the Gaussian mode-algorithm, the refractive index profiles and the thermal deformation of the crystal end faces are calculated (based on Alexandrite material parameters [15]). Figure 7(a) shows the temperature induced refractive index profile of FEA data (blue curve) and the parabolic fit (red curve) to the central part of the refractive index profile. The parabolic fit provides the thermally-induced lensing strength of the Alexandrite crystal, which is shown as a function of absorbed pump power in Fig. 7(b). At maximum absorbed pump power (10.3 W) used in the experimental laser system, the lens power is ~20 dioptres, corresponding to focal length 50 mm, indicating the strong lensing for the small pump radius size used (w_x =70 μm; w_y =63 μm).

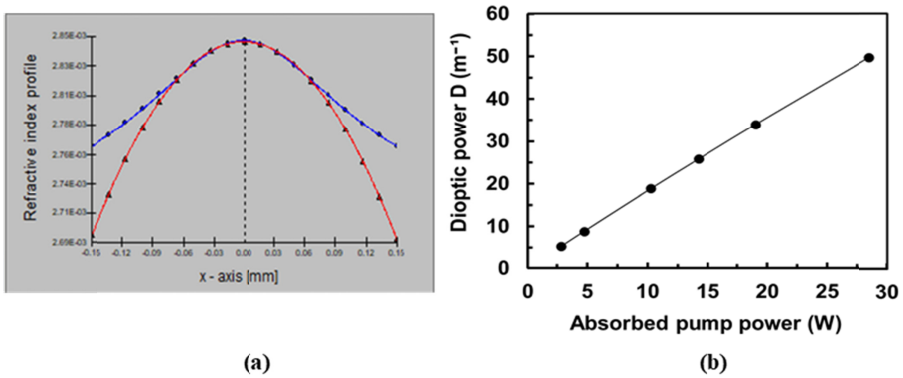

Fig. 7. (a) Temperature induced refractive index profile of FEA results for diode-pumped Alexandrite crystal (blue curve) and parabolic fit (red curve); (b) dioptic lensing power as function of absorbed pump power.

The primary design goal was to match the TEM_{00} laser mode size to the pump mode size which we take as nominal radius 70 µm and with pump region located predominantly within the first one or two millimetres of the input pump face (pump absorption depth ~ 1.7 mm). The overall design of the ring is chosen as a "displaced mode" cavity [15] as depicted in Fig. 8(a), with a mode waist much smaller in size than the pump size but whose displacement distance from the pump region allows the expansion of the laser mode to match to the pump beam waist size at the input pump face of the crystal. We define a designate distance, d, as the location of the laser mode waist with respect to the back face of the laser crystal as shown in Fig. 8(a). In the modelling, the two intracavity lenses L1 and L2 with identical focal length 100 mm had their position adjusted to provide the small waist with their positions defined as, d_1 and d_2 with respect to the two faces of the Alexandrite crystal, as shown in schematic diagram of Fig. 8(b).

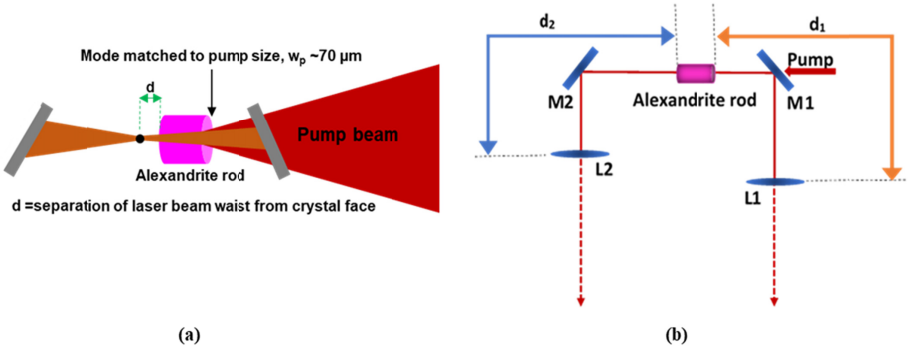

Fig. 8. (a) The "displaced mode" cavity design; and (b) adjustment of lens distances (d_1, d_2) to compensate the thermal lens (rod length 10 mm).

The graph of Fig. 9(a) shows the position of intracavity lenses, d_1 and d_2 that have been adjusted to satisfy the mode matching criteria for four different pump powers and using the corresponding thermal lensing strength given in Fig. 7(b). The lines fitted in the graph of Fig. 9(a) are extrapolations for d_1 and d_2 for intermediate pump powers. Figure 9(b) shows the variation of the laser mode size at the pump region as a function of pump power, for each of the four cases for d_1 and d_2 optimised at the given pump power in the key of the graph. The black dotted line in Fig. 9(b) shows the pump size that the laser mode is attempting to match for TEM_{00} operation. Figure 9(c) shows the waist distance parameter, d, as a function of absorbed pump power. The waist location is seen to move away from the pump region as the

pump power (and thermal lens strength) increases. At maximum absorbed pump power (10.3 W) in the experimental system, the distance, d, is 1.4 mm. The lens distance parameters, d_1 and d_2 (see Fig. 9(a)) are inter-related to waist location, d. The increase in, d, is achieved by increase in L2 arm length, d_2 but also, less obviously, to increase in L1 lens distance, d_1 since the total lensing in the L1 lens arm is a combination of lens L1 and the increasing thermal lensing strength in the laser crystal (Fig. 7(b)).

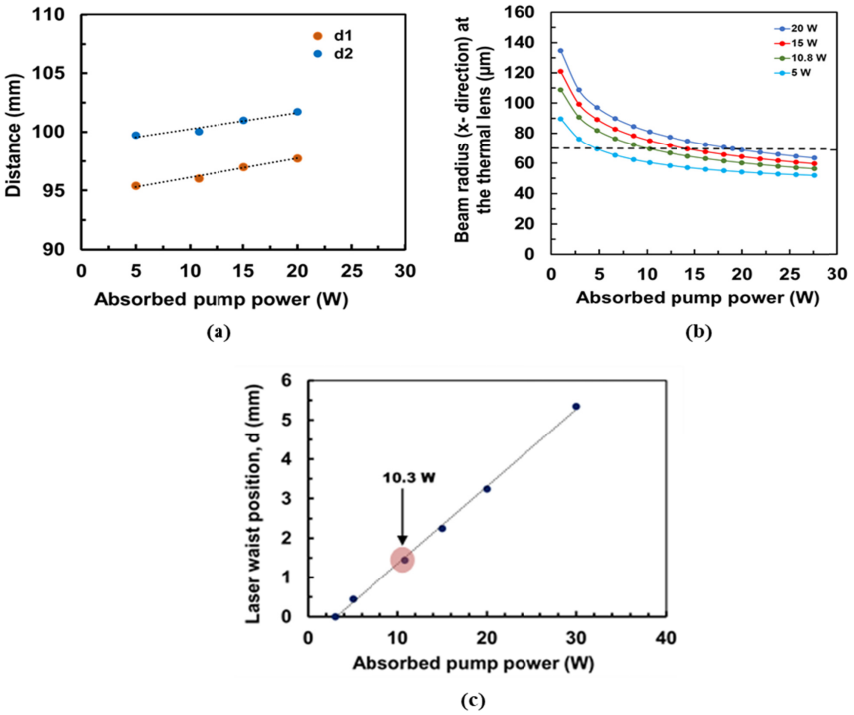

Fig. 9. (a) The lens distance parameters, d_1 and d_2, against absorbed pump power; (b) pump-dependent variation of laser TEM_{00} mode beam radius at the thermal lens for lens parameters (d_1, d_2) optimised at given pump power (black dotted line indicates pump size, wp ~70 μm, the target for laser mode matching); (c) displaced beam waist position, d, at different pump powers.

3.2 Experimental Alexandrite unidirectional ring laser results

In the experimental unidirectional Alexandrite ring laser shown in Fig. 6, the output coupler reflectivity was 99.2%. The total cavity length was 416 mm, with a compact rectangular cavity footprint 148 × 60 mm.

Figure 10(a) shows the unidirectional ring laser output power versus absorbed pump power. An output power of 700 mW was produced in an excellent near diffraction-limited TEM_{00} beam quality M^2_x =1.07 and M^2_y =1.06. The laser slope efficiency was 13% and the threshold pump power was 5.2 W. For comparison, the equivalent laser output power curve for an astigmatic bow-tie unidirectional ring cavity with Brewster-cut Alexandrite crystal [15] is shown in Fig. 10(b). The non-astigmatic ring is seen to have better spatial quality than the previous astigmatic ring not only in absolute terms, but also its ability to maintain this quality throughout the pump power range. On the other hand, the astigmatic ring in Fig. 10(b) is seen to have erratic power fluctuation and variation in spatial quality along its power curve due to the astigmatic pump-induced lensing in the Alexandrite laser crystal. There is a reduction in overall power, 700 mW, from the non-astigmatic ring laser, whilst the astigmatic ring output was 1.05 W. This power reduction is accountable due to a higher pump threshold caused by

higher overall intracavity loss, although it is noted that the laser slope efficiency 13% of the non-astigmatic ring laser is higher than the astigmatic ring which was only 11%.

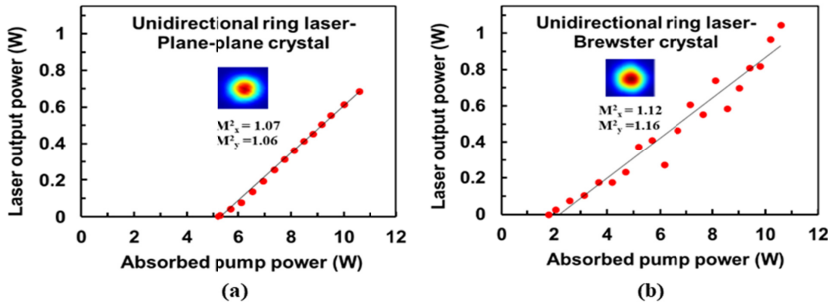

Fig. 10. Laser output power against absorbed pump power for the unidirectional Alexandrite ring laser under single-frequency operation; (a) non-astigmatic rectangular cavity (slope efficiency 13%) and output power of 0.7 W (this work) and (b) astigmatic bow-tie cavity (slope efficiency 11%) and output power of 1.05 W [15].

The non-astigmatic ring laser was wavelength tuned using the intracavity 1 mm thick BiFi quartz plate. The wavelength tuning results in Fig. 11(a) show the tuning range from 748 nm to 773 nm. Some of the limitation on the tuning range was due to the strongly reduced reflectivity of the OC at wavelengths longer than about 760 nm, as evident from the OC spectral reflectivity curve in Fig. 11(b).

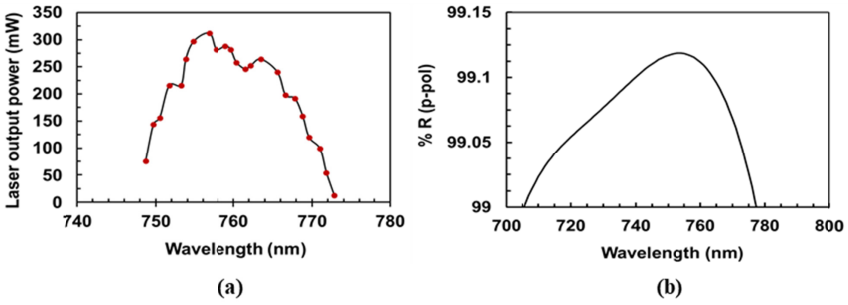

Fig. 11. (a) Wavelength tuning curve for the unidirectional Alexandrite ring laser, (b) spectral reflectivity curve of the output coupler, OC.

The spectrum of the unidirectional ring laser was investigated with a low resolution (~0.5 nm) spectrometer in Fig. 12(a) and by analysing the ring pattern of the laser output passed through a solid Fabry-Pérot (FP) etalon shown in Fig. 12(b).

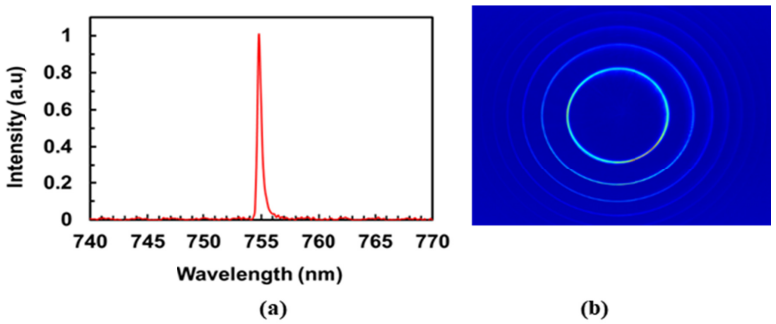

Fig. 12. (a) Spectrum of CW diode-pumped Alexandrite non-astigmatic unidirectional ring laser at peak wavelength 754.6 nm, (b) Spectral ring pattern from a Fabry-Pérot etalon showing single-longitudinal mode operation.

For the optical path length of the laser cavity ~430 mm (accounting for refractive indices of intracavity elements) the longitudinal mode spacing is ~700 MHz. The FP used in this experiment had a free spectral range of 6.9 GHz and finesse of 50 that correspond to a resolving power ~140 MHz, which means longitudinal modes can be well resolved. The single ring per FP free spectral range in Fig. 12(b) shows that the laser is running in a pure single-longitudinal-mode. To the best of our knowledge, this is the first demonstration of wavelength-tunable unidirectional single-longitudinal-mode operation of a CW diode-pumped Alexandrite ring laser with a non-astigmatic resonator design.

4. Conclusion

The outcome of this work is the design and successful operation of a non-astigmatic Alexandrite laser that operates with wavelength tunability and single-longitudinal-mode. One of the goals was to investigate whether this design could be a simpler suitable alternative to the more complex laser design with astigmatic Brewster-cut crystal and angled curved mirrors. The results of its operation have demonstrated achievement of a higher spatial quality TEM_{00} mode and over the full pump range, rather than the more complex behavior due to the asymmetric pump-induced lensing in the Brewster-cut crystal of the astigmatic design [15].

We have developed a non-astigmatic unidirectional Alexandrite ring laser design utilising non-astigmatic intracavity optical elements at normal incidence. Numerical modelling of a "displaced mode" ring cavity design is performed with ABCD Gaussian propagation software and numerical finite element analysis for incorporation of pump-dependent thermal lensing in the Alexandrite laser crystal. The modelling theory is used to optimise the TEM_{00} mode-matching cavity configuration by adjusting the relative distances of the intracavity lenses from the laser crystal and the laser mode waist location for varying thermal lens strength. An experimental demonstration is performed of a wavelength-tunable unidirectional Alexandrite ring laser in the non-astigmatic cavity design. The laser produced 700 mW of CW output power with a slope efficiency of 13%. Excellent TEM_{00} beam quality with M^2 <1.1 is achieved across the whole pump power range. Spectral analysis shows SLM output and wavelength tuning from 748 nm to 773 nm, limited by the spectral reflectivity of the cavity optics. To the best of our knowledge, this is the first wavelength-tunable SLM operation of a unidirectional Alexandrite ring system in the non-astigmatic cavity regime.

One of the goals to show if a simpler non-astigmatic design could be used as a suitable alternative to the more complex astigmatic design has been demonstrated. The non-astigmatic design allowed both a simpler modelling and achievement of a higher spatial quality TEM_{00} mode over a wider pump range. Although it may be possible to achieve the same performance in the astigmatic cavity, the adjustment compensation is more complex to accomplish for both the horizontal and vertical axis at the same time, as the thermal lens changes. The physical footprint size of both cavities was similarly compact. The non-astigmatic cavity had a higher laser slope efficiency but lower output power due to higher losses and smaller tuning range due to poorer spectral coatings of cavity optics. These latter issues could be accounted for, in principle, with higher quality optical coatings in future development of the non-astigmatic laser. However, if very wide wavelength tuning is required (e.g. as in multi-hundred nanometer tuning in Ti:Sapphire), the Brewster-cut crystal with no coating, and high reflectivity mirrors of the astigmatic cavity design, has spectral tuning advantages. For the relatively limited tuning of Alexandrite (sub-hundred nanometer or multi-ten nanometers) this issue is less problematic and the non-astigmatic design with suitably AR-coated Alexandrite crystal and intracavity lenses is a viable alternative. Future work suggests improvements be made to efficiency and tuning performance of the non-astigmatic laser design with the inclusion of better-quality optics and intra-cavity elements with reduced insertion losses, and more consideration of operation at a higher Alexandrite crystal temperature. The results obtained in this experiment provide an insight into the design

parameters for optimum performance as needed for high-spectral precision applications in remote sensing (Lidar), spectroscopy or quantum technologies.

5. Funding, acknowledgments, and disclosures

5.1 Funding

Engineering and Physical Sciences Research Council (EPSRC) (EP/R00420X/1); Innovate UK (132531).

5.2 Acknowledgments

We thank M Squared Lasers Ltd. for collaboration in this work. We also thank S. Johnson and M. Kehoe of the Optics Mechanical Workshop at Imperial College London for manufacturing holders and mounts for the laser cavity components.

5.3 Disclosures

The authors declare that there are no conflicts of interest related to this article.

6. References

1. P. Arora, R. Sarkar, V. K. Garg and L. Arya. “Lasers for treatment of melasma and post-inflammatory hyperpigmentation”. J Cutan Aesthet Surg. 5, 93-103 (2012).
2. P. Bakule, P. E. G. Baird, M. G. Boshier, S. L. Cornish, D. F. Heller, K. Jungmann, I. C. Lane, V. Meyer, P. H.G. Sandars, W. T. Toner, M. Towrie, and J. C. Walling, “A chirp-compensated, injection-seeded alexandrite laser,” Appl. Phys. B 71, 11–17 (2000).
3. V. Wulfmeyer and J. Bösenberg, “Single-mode operation of an injection-seeded alexandrite ring laser for application in water-vapor and temperature differential absorption lidar,” Opt. Lett. 21, 1150–1152 (1996).
4. J. W. Kuper, T. Chin, and H. E. Aschoff, “Extended Tuning Range of Alexandrite at Elevated Temperatures,” in Advanced Solid State Lasers, Vol. 6 of OSA Proceedings Series (Optical Society of America, 1990), paper CL3.
5. J. Walling, O. Peterson, H. Jenssen, R. Morris, and E. O’Dell, “Tunable Alexandrite lasers,” IEEE J. Quantum Electron. 16, 1302–1315 (1980).
6. J. Walling, D. F. Heller, H. Samelson, D. J. Harter, J. Pete, and R. C. Morris, “Tunable alexandrite lasers: Development and performance,” IEEE J. Quantum Electron. 21, 1568–1581 (1985).
7. M. Fibrich, J. Sulc, and H. Jelinkova, “Alexandrite microchip lasers,” Opt. Express 27, 16975-16982 (2019).
8. M. Damzen, G. Thomas, A. Teppitaksak, and A. Minassian, “Progress in diode-pumped Alexandrite lasers as a new resource for future space lidar missions,” in International Conference on Space Optics (2014).
9. R. Scheps, B. M. Gately, J. F. Myers, J. S. Krasinski, and D. F. Heller, “Alexandrite laser pumped by semiconductor lasers,” Appl. Phys. Lett. 56, 2288–2290 (1990).
10. R. Scheps, J. F. Myers, T. R. Glesne, and H. B. Serreze, “Monochromatic end-pumped operation of an Alexandrite laser,” Opt. Commun. 97, 363–366 (1993).
11. M. J. Damzen, G. M. Thomas, and A. Minassian, “Diode-side-pumped Alexandrite slab lasers,” Opt. Express 25, 11622-11636 (2017).
12. A. Teppitaksak, A. Minassian, G. M. Thomas, and M. J. Damzen, “High efficiency >26 W diode end-pumped Alexandrite laser,” Opt. Express 22, 16386–16392 (2014).
13. W. R. Kerridge-Johns and M. J. Damzen, “Temperature effects on tunable cw Alexandrite lasers under diode end-pumping,” Opt. Express 26, 7771–7785 (2018).
14. A. Munk, B. Jungbluth, M. Strotkamp, H.-D. Hoffmann, R. Poprawe, J. Höffner, and F.-J. Lübken, “Diode-pumped alexandrite ring laser in single-longitudinal mode operation for atmospheric lidar measurements,” Opt. Express 26, 14928–14935 (2018).
15. X. Sheng, G. Tawy, J. Sathian, A. Minassian, and M. J. Damzen, “Unidirectional single-frequency operation of a continuous-wave Alexandrite ring laser with wavelength tunability,” Opt. Express 26, 31129-31136 (2018).
16. H. Kogelnik, E. P. Ippen, A. Dienes, and C. V. Shank, “Astigmatically compensated cavities for CW dye lasers,” IEEE J. Quantum Electron. 8, 373–379 (1972).
17. D. M. Kane, “Astigmatism compensation in off-axis laser resonators with two or more coupled foci,” Opt. Commun. 71, 113–118 (1989).
18. K. Lin, Y. Lai, and W. Hsieh, “Simple analytical method of cavity design for astigmatism-compensated Kerr-lens mode-locked ring lasers and its applications,” J. Opt. Soc. Am. B 12, 468-475 (1995).
19. W. Qiao, Z. Xiaojun, W. Yonggang, S. Liqun, and N. Hanben, “A simple method for astigmatic compensation of folded resonator without Brewster window,” Opt. Express 22, 2309-2316 (2014).
20. C. Ramírez-Guerra, J. A. Moreno-Larios, M. Rosete-Aguilar, and J. Garduño-Mejía, “Mode-coupling enhancement by pump astigmatism correction in a Ti:Sapphire femtosecond laser,” Appl. Opt. 55, 9889-9894 (2016).

21. M. Strotkamp, A. Munk, B. Jungbluth, H. D. Hoffmann, and J. Höffner, “Diode-pumped Alexandrite laser for next generation satellite-based earth observation lidar,” CEAS Space J. 11, 413–422 (2019).